

# Influences of dynamic material properties of slab track components on the train-track vibration interactions

Li, Ting; Su, Qian; Kaewunruen, Sakdirat

*Citation for published version (Harvard):*

Li, T, Su, Q & Kaewunruen, S 2020, 'Influences of dynamic material properties of slab track components on the train-track vibration interactions', *Engineering Failure Analysis*.

[Link to publication on Research at Birmingham portal](#)

## General rights

Unless a licence is specified above, all rights (including copyright and moral rights) in this document are retained by the authors and/or the copyright holders. The express permission of the copyright holder must be obtained for any use of this material other than for purposes permitted by law.

- Users may freely distribute the URL that is used to identify this publication.
- Users may download and/or print one copy of the publication from the University of Birmingham research portal for the purpose of private study or non-commercial research.
- User may use extracts from the document in line with the concept of 'fair dealing' under the Copyright, Designs and Patents Act 1988 (?)
- Users may not further distribute the material nor use it for the purposes of commercial gain.

Where a licence is displayed above, please note the terms and conditions of the licence govern your use of this document.

When citing, please reference the published version.

## Take down policy

While the University of Birmingham exercises care and attention in making items available there are rare occasions when an item has been uploaded in error or has been deemed to be commercially or otherwise sensitive.

If you believe that this is the case for this document, please contact [UBIRA@lists.bham.ac.uk](mailto:UBIRA@lists.bham.ac.uk) providing details and we will remove access to the work immediately and investigate.

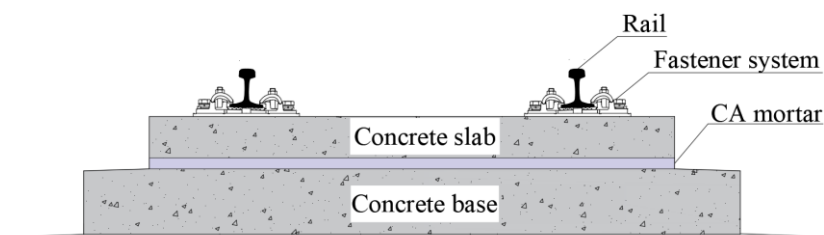


30 reference and recommendation for adopting suitable and realistic material properties of  
31 high-speed slab tracks in practice.

32 **Keywords:** dynamic material properties; strain-rate effect; train-track interactions; high-speed  
33 railway; finite element model

## 34 1. Introduction

35 Slab tracks have become a prevalent trend for highspeed railways throughout the world  
36 because of its advantages for higher stability, lower track deformation, and much lower  
37 maintenance compared with ballasted tracks [1, 2]. In China, the operating mileage of  
38 highspeed railway networks has reached 29,000 km by the end of 2018, and most of the track  
39 structures are indeed slab tracks [3, 4]. The China Railway Track System (CRTS) I slab track  
40 is a typical non-ballasted track structure, which has been adopted in many high-speed  
41 railways in China, such as Qinhuangdao-Shenyang passenger dedicated line,  
42 Shanghai-Nanjing intercity railway line, and Chengdu-Mianyang-Leshan High-speed railway  
43 line. This slab track is mainly composed of the CHN60 rail (Chinese standard rail with the rail  
44 mass 60 kg/m), the WJ-7B fastener system, the concrete slab, the cement-emulsified asphalt  
45 (CA) mortar layer, and the concrete base, as illustrated in Figure 1.



46

47

Figure 1 Section of the CRTS I slab track

48 Material properties of the slab track are an essential element for designing and predicting  
49 the dynamic performance of the high-speed railway under dynamic train loads. This dynamic  
50 performance is often the governing requirement as part of serviceability limit states for track  
51 systems. In practice, the elastic constitutive model of slab tracks is often used in design and  
52 numerical predictions. Material properties of track components are the key factors for the  
53 constitutive models, mainly consisting of the mass density, the modulus of elasticity, and the  
54 Poisson's ratio for solid elements, and the stiffness and damping for spring-dashpot elements.

55 In order to determine vehicle-track interactions, the designed static material properties of the  
56 slab track components are normally adopted in most previous studies and these properties are  
57 mainly measured from the quasi-static loading tests in laboratories [5-7]. For example, the  
58 modulus of elasticity of the concrete slab is  $3.6 \times 10^{10}$  Pa, which is determined by the  
59 compressive strength test for the C60 concrete, and the test loading is simply static [7]. The  
60 stiffness of the rail pads in WJ-7B fastener system is  $2.5 \times 10^7$  N/m, which is also measured  
61 from the static loading tests [7]. These material properties are the static properties obtained  
62 from benchmarking test requirements. In real life, a train will apparently impart dynamic  
63 excitations onto slab tracks. Especially when the train speed becomes faster, the vibration  
64 induced by the dynamic train loads will cause a lot of defects to track components [4, 8-10].  
65 Thus, appropriate material properties of slab track components shall be taken into account  
66 when performing dynamic interaction simulations. Several studies have shown that the  
67 properties of various materials such as concrete and cement-based materials under dynamic  
68 loads will be magnified compared with the properties under static or quasi-static loads,  
69 especially for the modulus of elasticity [11-13]. For rails, it is a composite metal material with  
70 chemical elements like C, Mn, Si, P, S, and so on. The modulus of elasticity of rail is not  
71 sensitive to the dynamic excitation so that it will not change much under dynamic train loads  
72 [14]. However, it is well known that the concrete is a strain-rate dependent material under  
73 dynamic loads, indicating the modulus of elasticity of concrete will be increased significantly  
74 with strain rates [15-18]. The CA mortar is also sensitive to strain rates under dynamic loads  
75 [19-22]. Zeng et al. [23] carried out an experiment to study the dynamic properties of CA  
76 mortar in CRTS I slab track and the dynamic modulus of elasticity of CA mortar could be  
77 increased by 75% of the static values. As the main elastic elements to absorb the vibration  
78 energy, the soft rail pads are normally installed in high-speed railways [24, 25]. The static  
79 stiffness of rail pads is 20-30 kN/mm according to the design code of high-speed railways in  
80 China. However, the dynamic stiffness of rail pads is not easy to be determined because the  
81 rail pad is a frequency- and temperature- dependent material in practice [26]. Hopefully, the  
82 rail pads are normally simplified as the spring elements in numerical simulations and the  
83 constant values have been normally adopted [27]. The dynamic stiffness of rail pads under  
84 cyclic loads is around 1.3-2 times the static stiffness for WJ-7B fastener system [28, 29]. It is

85 noted that other material properties such as the mass density and the Poisson's ratio are not  
86 sensitive to the dynamic strain rates, whilst the damping must be determined by the dynamic  
87 loading tests [30]. Therefore, relatively among all of the elastic materials properties, the  
88 modulus of elasticity and the stiffness are the most sensitive properties to the dynamic  
89 excitations in slab tracks.

90 Dating back to 1978, Birmann [31] was the first to study the dynamic modulus of  
91 elasticity of the ballasted track with regard to high speeds through simulations. However, at  
92 that time, the train and track were just simplified using a multi-body simulation idealization as  
93 the mass and spring models due to the low computational efficiency, so the train-track  
94 vibration interactions like wheel-rail contact force and dynamic stress of the track  
95 components cannot be acquired. Nowadays, the 3D coupled vehicle-track numerical model  
96 has become an efficient solution to study the complicated dynamic performance of the  
97 high-speed railways [27, 32]. However, the static material properties of the slab track  
98 components are still adopted on a large scale in many numerical models [33-36]. For example,  
99 Zhu et al. [33, 34] developed a 3D coupled vehicle-track model to study the deterioration of  
100 the slab track by using static properties. Xu et al. [35] also used the static properties in the  
101 coupled vehicle-track model to analyze the stochastic vibrations. Sun et al. [36] analyzed the  
102 track-bridge vibration by using static properties of the slab tracks. In addition, some scholars  
103 like Zhai et al., Lei et al., and Ren et al., [37-39] combined the dynamic stiffness of rail pads  
104 with still static modulus of elasticity for concrete and CA mortar in their coupled  
105 vehicle-track models to analyse the dynamic performance, but nearly nobody explains why  
106 both static and dynamic material properties were used in the one simulation model under  
107 dynamic excitations. To the authors' knowledge, there are no previous studies investigating  
108 the influences of the dynamic material properties of slab track components on train-track  
109 vibration interactions. It is still questionable at large whether it is appropriate for predicting  
110 the dynamic performance of the railway by using static material properties and whether there  
111 is a need to consider fully the dynamic properties of slab track components in the coupled  
112 vehicle-track numerical models under actual dynamic train excitations.

113 In order to investigate the influences of the dynamic material properties of the slab track  
114 components on the vibration responses of the train and track, a nonlinear 3D coupled

115 vehicle-slab track numerical model has been developed based on the multi-body simulation  
116 principle and finite element method using LS-DYNA. Three types of material properties of  
117 slab track components have been adopted for the parametric studies: static stiffness for rail  
118 pads and static modulus of elasticity for concrete and CA mortar, dynamic stiffness for rail  
119 pads and static modulus of elasticity for concrete and CA mortar, and dynamic stiffness for  
120 rail pads and dynamic modulus of elasticity for concrete and CA mortar. The 3D model has  
121 been validated firstly. Then, the magnification effect of the dynamic modulus of elasticity has  
122 been analyzed. Accordingly, the vibration of the vehicle, the wheel-rail contact force, the  
123 vibration responses of the slab tracks can be determined for various train speeds from 10 km/h  
124 to 400 km/h, taking into account the three types of material properties. Ultimately, the  
125 deviation coefficients, which present the influence of the properties on vibration responses,  
126 have been evaluated to provide the evidence and recommendation for adopting suitable and  
127 realistic material properties of high-speed slab tracks in practice.

## 128 **2. Material properties of the slab track**

129 The material properties of the slab track are different when they are measured by either  
130 quasi-static or dynamic loading tests. When the properties are measured by quasi-static  
131 loading tests, the material properties are named as static properties in this paper. In contrast,  
132 when they are measured by dynamic loading tests, the properties are named as dynamic  
133 properties. The static and dynamic material properties of CRTS I slab track are presented in  
134 the following parts.

### 135 **2.1 Static properties of the slab track**

136 The static material properties of the CRTS I slab track components can be found in [7],  
137 as shown in Table 1. The stiffness of rail pads and the moduli of elasticity of the concrete slab,  
138 CA mortar, and concrete base are determined from the quasi-static loading tests.

139 Table 1 Static properties of the CRTS I slab track

Properties	Values
Mass density of the rail ( $\text{kg/m}^3$ )	7830

Modulus of elasticity of the rail (Pa)	$2.059 \times 10^{11}$
Poisson's ratio of the rail	0.3
Stiffness of the rail pads (N/m)	$2.5 \times 10^7$
Damping of the rail pads (N.s/m)	$7.5 \times 10^4$
Mass density of the concrete slab ( $\text{kg/m}^3$ )	2500
Modulus of elasticity of the concrete slab (Pa)	$3.6 \times 10^{10}$
Poisson's ratio of the concrete slab	0.2
Mass density of the CA mortar ( $\text{kg/m}^3$ )	1600
Modulus of elasticity of the CA mortar (Pa)	$3 \times 10^8$
Poisson's ratio of the CA mortar	0.2
Mass density of the concrete base ( $\text{kg/m}^3$ )	2500
Modulus of elasticity of the concrete base (Pa)	$3.25 \times 10^{10}$
Poisson's ratio of the concrete base	0.2

---

## 140 **2.2 Dynamic stiffness of the rail pads**

141 The rail pads play an important role in reducing vibration on track components. They are  
142 normally made out of rubber, high-density polyethylene (HDPE), thermoplastic polyester  
143 elastomer (TPE), and ethylene vinyl acetate (EVA) [24, 25]. The rail pads also come in a wide  
144 range of stiffness due to different types of materials. So that the stiffness of rail pads can be  
145 classified as soft, medium, stiff, very stiff, and extremely stiff [25]. However, there are no  
146 standard classification values for the rail pads around the world since the properties vary in  
147 relation to track characteristics. According to [25], the stiffness of soft pads is less than 80 or  
148 130 kN/mm, and the soft pads are normally used in WJ-7B fastener system, which is widely  
149 adopted in high-speed railways in China.

150 According to the literature reviewed, the dynamic stiffness of rail pads is temperature-  
151 and frequency-dependent, and it is also sensitive to the preloads when the stiffness is tested in  
152 the laboratory [24, 26, 40]. Therefore, the dynamic stiffness of rail pads is a complicated  
153 parameter in practice. Hopefully, in order to describe the viscoelasticity characteristics of rail  
154 pads, the rail pads are normally simplified as the spring and dashpot elements, so that the

155 constant values are normally used in the numerical simulation models to describe the dynamic  
 156 characteristics of rail pads [27, 32].

157 When the constant value is used, the dynamic stiffness of rail pads is normally 1.3-2  
 158 times the static value according to previous studies [28, 29]. For the coupled vehicle-track  
 159 model, many researchers used two times the static stiffness to represent the dynamic  
 160 characteristics of rail pads [28, 37-39]. Since the static stiffness of rail pads in this paper is 25  
 161 kN/mm, the dynamic stiffness of rail pads is determined as 50 kN/mm for CRTS I slab track  
 162 in this study, as shown in Table 2.

163 Table 2 Stiffness of the rail pads in CRTS I slab track

-	Static stiffness	Dynamic stiffness
Values (kN/mm)	25	50

### 164 2.3 Strain-rate-dependent moduli of elasticity of the concrete and CA mortar

165 The effect of strain-rate on modulus of elasticity for concrete under dynamic loads has  
 166 been studied by many researchers [41, 42]. The Comite Euro-International Du Beton (CEB)  
 167 has put forward the strain-rate enhancement factors for the compressive and tensile modulus  
 168 of elasticity as follows [30]:

$$169 \quad \eta_c = \frac{E_d}{E_s} = \left(\frac{\dot{\epsilon}}{\dot{\epsilon}_{sc}}\right)^{0.026} \quad (1)$$

$$170 \quad \eta_t = \frac{E_d}{E_s} = \left(\frac{\dot{\epsilon}}{\dot{\epsilon}_{st}}\right)^{0.016} \quad (2)$$

171 Where  $\eta_c$  and  $\eta_t$  are the compressive and tensile strain-rate enhancement factors,  
 172 respectively;  $E_d$  and  $E_s$  are the dynamic and static modulus of elasticity, respectively;  $\dot{\epsilon}$   
 173 is the effective strain-rate of concrete under dynamic loads;  $\dot{\epsilon}_{sc}$  is the effective strain-rate of  
 174 concrete under compressive static loads, and it equals to  $30 \times 10^{-6}$  /s; and  $\dot{\epsilon}_{st}$  is the effective  
 175 strain-rate of concrete under tensile static loads, and it equals to  $3 \times 10^{-6}$  /s. Note that the  
 176 relationship between the effective strain-rate and the strain-rate components in different  
 177 directions can be calculated as follows:



$$\dot{\epsilon} = \sqrt{\frac{2}{3}} \{\dot{\epsilon}_{ij} \dot{\epsilon}_{ij}\}^{1/2} = \sqrt{\frac{2}{3}} \{\dot{\epsilon}_1^2 + \dot{\epsilon}_2^2 + \dot{\epsilon}_3^2\}^{1/2} \quad (3)$$

$$= \frac{2}{3} \left\{ \frac{1}{2} [(\dot{\epsilon}_x - \dot{\epsilon}_y)^2 + (\dot{\epsilon}_y - \dot{\epsilon}_z)^2 + (\dot{\epsilon}_z - \dot{\epsilon}_x)^2] + \frac{3}{4} (\dot{\gamma}_{xy}^2 + \dot{\gamma}_{yz}^2 + \dot{\gamma}_{zx}^2) \right\}^{1/2}$$

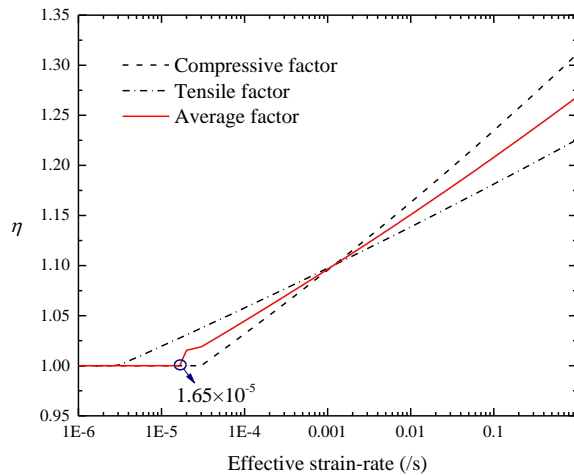
178

179 Where  $\dot{\epsilon}_1, \dot{\epsilon}_2,$  and  $\dot{\epsilon}_3$  are the principal strain-rates;  $\dot{\epsilon}_x, \dot{\epsilon}_y,$  and  $\dot{\epsilon}_z$  are the normal strain-rates in  
 180 three directions, and  $\dot{\gamma}_{xy}, \dot{\gamma}_{yz},$  and  $\dot{\gamma}_{zx}$  are the shear strain-rates in three directions.

181 It is quite difficult to determine which parts of the concrete slab and concrete base are  
 182 under compressive- or tensile- state when the train passes by since the dominant mechanical  
 183 state changes typically with time. By referring to the method for strain-rate enhancement in  
 184 Winfrith concrete model [41, 42], the average strain-rate enhancement factor is used for  
 185 concrete slab and concrete base:

$$\eta_{aver} = \frac{1}{2} (\eta_c + \eta_t) \quad (4)$$

186  
 187 The compressive-, tensile-, and average- enhancement factors are calculated with the  
 188 effective strain-rate, as shown in Figure 2. When the strain-rate changes from  $1 \times 10^{-6}$  /s to 1 /s,  
 189 the maximum deviation between compressive factor and tensile factor is around 7% at 1 /s,  
 190 indicating that the average enhancement factor will not cause a significant deviation to the  
 191 dynamic analysis. Note that the static effective strain-rates for compression and tension are  
 192  $3 \times 10^{-5}$  /s and  $3 \times 10^{-6}$  /s, respectively, when the effective strain-rate is lower than the static  
 193 values, the enhancement factor is set to equal to 1. And the average static effective strain-rate  
 194 is  $1.65 \times 10^{-5}$  /s.

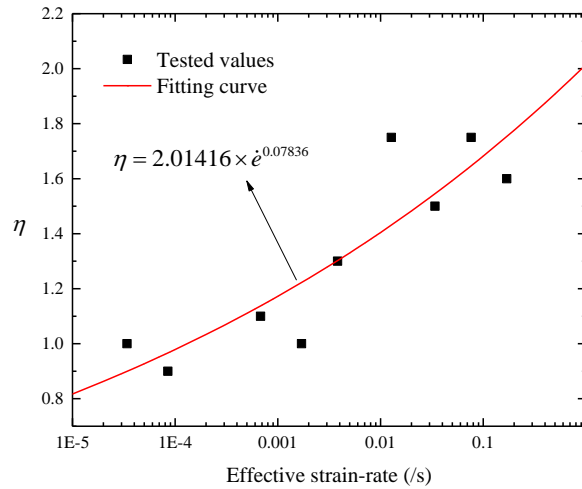


195

196 Figure 2 The strain-rate enhancement factors with effective strain-rate for concrete

197 According to [23], the strain-rate enhancement factor for modulus of elasticity of CA  
 198 mortar in CRTS I slab track can be acquired from the tested values, as shown in Figure 3. The  
 199 fitting curve is calculated as follows:

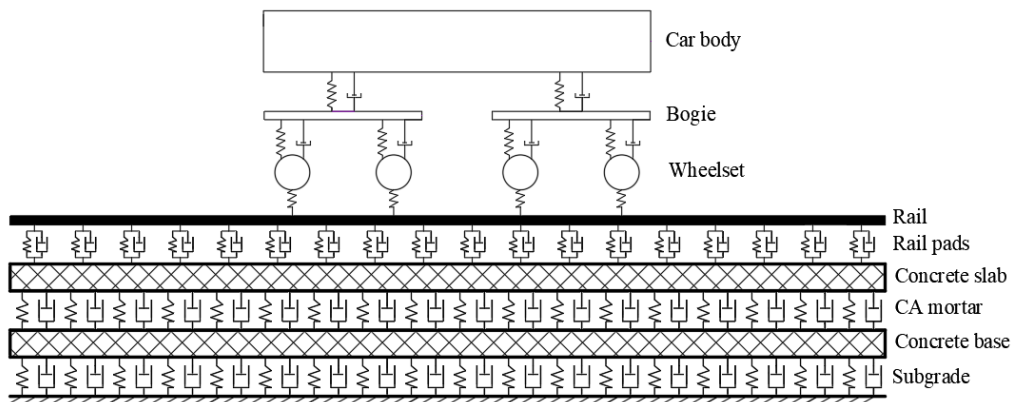
200 
$$\eta = 2.01416 \times e^{0.07836} \quad (5)$$



201  
 202 Figure 3 The strain-rate enhancement factor with effective strain-rate for CA mortar

203 **3. Development of the numerical model**

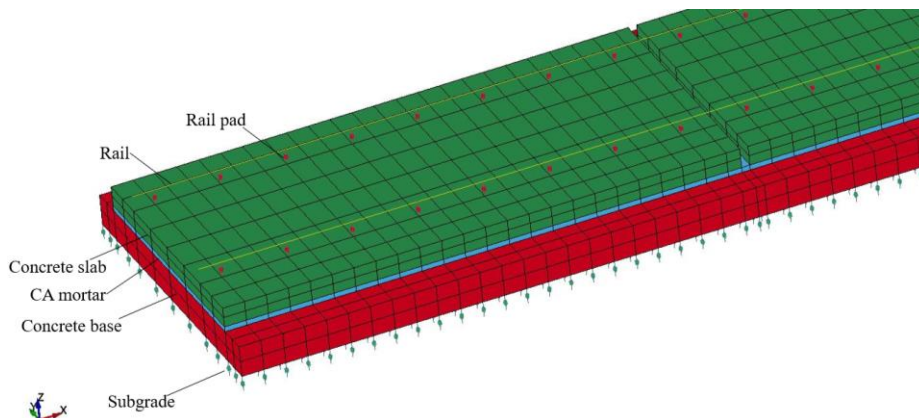
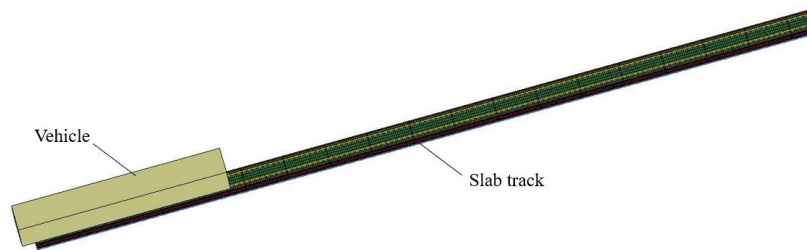
204 In order to investigate the influence of the dynamic material properties of the slab track  
 205 on the vibration responses of the train and track, a 3D coupled vehicle-slab track numerical  
 206 model has been developed, as shown in Figure 4. The vehicle is developed based on the  
 207 multi-body simulation principle, and the slab track is simulated based on the finite element  
 208 theory using the commercial software LS-DYNA.



209  
 210 Figure 4 The coupled vehicle-slab track numerical model

211 **3.1 Vehicle and slab track elements**

212 The vehicle consists of one car body, two bogies, four wheelsets, and two-stage  
213 suspension system. The car body, bogies, and wheelsets are simplified as rigid bodies using  
214 shell and beam elements. Each component of the vehicle is connected by the suspension  
215 springs and dashpots. The vehicle has a total 10 degrees of freedom, including the vertical and  
216 pitch motion of the car body, vertical and pitch motion of the bogies, and vertical motion of  
217 the wheelsets. The slab track is composed of rail, rail pads, concrete slab, CA mortar, and  
218 concrete base. The rail is modeled as Euler beam supported by rail pads, which are simulated  
219 as the spring and dashpot elements. The concrete slab, CA mortar, and concrete base are  
220 modeled by solid elements in order to acquire the complicated 3D mechanical state. And the  
221 subgrade is described as the spring-damping system, which is widely used in many simulation  
222 models [27, 35]. The whole model has 38,344 elements including beam, shell, solid, spring,  
223 and dashpot, as shown in Figure 5.



228 **Figure 5 The coupled vehicle-slab track model in LS-DYNA (a) Top view of the entire model**

229 **(b) Detailed slab track model**

230 **3.2 Wheel-rail contact theory**

231 The wheel-rail contact is developed by the built-in keywords in LS-DYNA: \*Rail\_Track  
 232 and \*Rail\_Train. Users can input the contact parameters like the stiffness of the wheel-rail  
 233 contact spring, the irregularity of the track, and so on.

234 The wheel-rail contact force can be calculated automatically by LS-DYNA based on the  
 235 following equation:

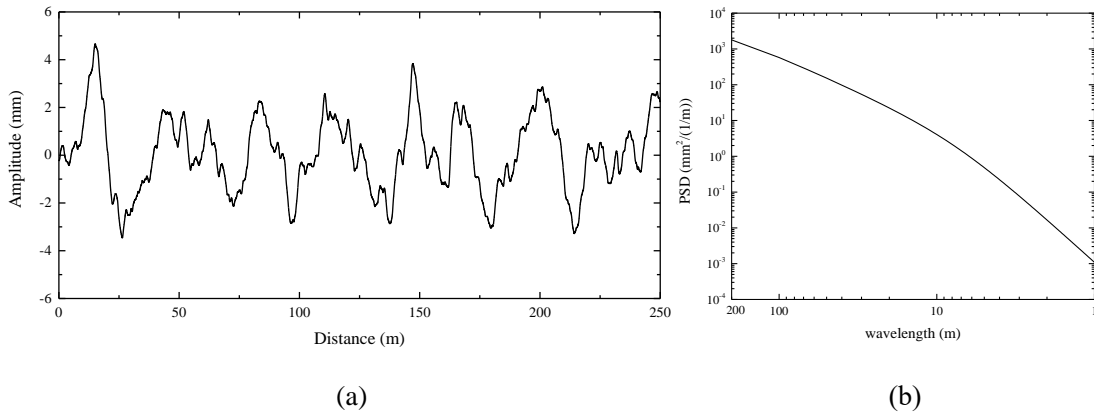
236 
$$F = K \times (Z_w - Z_r - \delta) \quad (6)$$

237 Where  $F$  is the wheel-rail contact force;  $K$  is the vertical stiffness of the wheel-rail contact  
 238 spring,  $K = 1.325 \times 10^9$  N/m in this study [38];  $Z_w$  is the vertical displacement of the wheel;  
 239  $Z_r$  is the vertical displacement of the rail; and  $\delta$  is the track irregularity.

240 The irregularity of the Germany high-speed low disturbance is used to excite the  
 241 wheel-rail interactions. The power spectrum density (PSD) function of the track irregularity is  
 242 calculated as follows:

243 
$$S_v(\Omega) = \frac{A_v \Omega_c^2}{(\Omega^2 + \Omega_r^2)(\Omega^2 + \Omega_c^2)} \quad (7)$$

244 Where  $S_v(\Omega)$  is the vertical power spectral density;  $A_v$  is the roughness constant  
 245 ( $A_v = 4.032 \times 10^{-7}$  m<sup>2</sup> · Rad/m);  $\Omega_c$  and  $\Omega_r$  are the cutoff frequency ( $\Omega_c = 0.8246$  rad/m ,  
 246  $\Omega_r = 0.0206$  rad/m); and  $\Omega$  is the spatial frequency of the irregularities. The PSD function  
 247 can be transformed into vertical irregularities along the longitudinal distance of the track by  
 248 means of a time-frequency transformation technique [14], as shown in Figure 6.



249  
 250 (a) (b)  
 251 Figure 6 Track irregularity (a) Track irregularity with distance (b) PSD with wavelength

### 252 **3.3 Material control**

253 When the static material properties of the slab track are used, the built-in keyword of  
254 001-ELASTIC is used for concrete slab, CA mortar, and concrete base. The mass density, the  
255 static modulus of elasticity, and the Poisson's ratio are needed to be input by users. Also, the  
256 keywords of S01-SPRING\_ELASTIC and S02-DAMPER\_VISCOUS are used to describe the  
257 static stiffness and the damping of rail pads.

258 When the dynamic stiffness of rail pads is considered, the keywords of  
259 S01-SPRING\_ELASTIC is still used but using the dynamic stiffness values for rail pads. In  
260 addition, when the strain-rate enhancement effect is considered, the keyword of  
261 019-STRAIN\_RATE\_DEPENDENT\_PLASTICITY is used for concrete slab, CA mortar, and  
262 concrete base. In this keyword, the yield stress and modulus of elasticity are needed as a  
263 function of the effective strain-rate. Note that the concrete and CA mortar are normally within  
264 the static stage under dynamic train loads, the yield stress of these materials can be set as a  
265 constant and high value which can protect the material from yield. The yield stress of concrete  
266 slab, CA mortar, and concrete base are set as 60 MPa, 5 MPa, and 40 MPa, respectively. As  
267 for the modulus of elasticity with effective strain-rate, it can be determined from Figure 2.

### 268 **3.4 Numerical solution**

269 The vehicle moves at a constant speed over the rail after the dynamic relaxation. The  
270 explicit central difference method is used to integrate the motion equations of the coupled  
271 vehicle and track model by LS-DYNA.

## 272 **4. Model validation**

273 The Suining-Chongqing railway in China was constructed as a test section to analyze the  
274 dynamic performance of slab tracks. Many researchers have conducted field tests to acquire  
275 the vibration responses of the vehicle and slab track [43-46]. The passenger vehicle which  
276 was running on this railway was "Changbai Mountain", which is an old vehicle type in China.  
277 Nowadays, the primary vehicle is the China Railway High-speed (CRH) 2 Electric Multiple

278 Unit (EMU) train, and properties of the CRH 2 EMU train are shown in Table 3 [39].

279 Table 3 Properties of the CRH 2 EMU train

Properties	Values
Mass of the car body (kg)	39,600
Mass of the bogie (kg)	3,500
Mass of the wheelset (kg)	2,000
Inertia of pitch motion of the car body(kg.m <sup>2</sup> )	1.283×10 <sup>5</sup>
Inertia of pitch motion of the bogie(kg.m <sup>2</sup> )	2,592
Stiffness of the primary suspension (N/m)	1.176×10 <sup>6</sup>
Damping of the primary suspension (N.s/m)	1.96×10 <sup>4</sup>
Stiffness of the secondary suspension (N/m)	1.89×10 <sup>6</sup>
Damping of the secondary suspension (N.s/m)	4×10 <sup>4</sup>
Length between the center of bogies (m)	17.5
Wheelbase for the bogie (m)	2.5
Radius of the wheel (m)	0.43

280

281 The field test results were recorded every time the “Changbai Mountain” or CRH 2 EMU  
282 train passes by the test section, and the train speed was 160-220 km/h. Cai and Zhai et al. [47]  
283 have conducted a numerical simulation to study the vibration responses of the slab track at  
284 200 km/h. In their numerical model, the “Changbai Mountain” vehicle was used and the track  
285 irregularity measured from Qinhuangdao-Shenyang railway was used to excite the train-track  
286 interactions. As for the material properties of the slab track in their model, the dynamic  
287 stiffness of the rail pads and the static modulus of elasticity are used. In order to validate the  
288 simulation results calculated from the model developed in this paper, the CRH 2 EMU train  
289 and the irregularity of Germany high-speed low disturbance are adopted. Three types of  
290 material properties are considered: Case 1: using static stiffness of rail pads and static  
291 modulus of elasticity of concrete and CA mortar; Case 2: using dynamic stiffness of rail pads  
292 and static modulus of elasticity of concrete and CA mortar; Case 3: using dynamic stiffness of  
293 rail pads and dynamic modulus of elasticity of concrete and CA mortar. The vibration

294 responses are calculated at 200 km/h in order to compare the results with field tests and  
 295 simulations. The validation results are shown in Table 4.

296 Table 4 Validation results

	Field test results [43-46]	Simulation results from Cai et al [47]	Simulation results from this paper		
			Case 1	Case 2	Case 3
Wheel-rail contact force (kN)	81-116	98.7	85.4	95.3	96.3
Rail pad force (kN)	14.4-65.8	37.648	27.4	34.7	35.1
Displacement of the rail (mm)	0.3-0.88	0.827	1.243	0.878	0.863
Displacement of the slab (mm)	0.081-0.284	0.283	0.189	0.254	0.240

297 The field test results have a certain range for every vibration response due to the different  
 298 train types and speeds and so on. The simulation results from Cai et al. [47] are within the  
 299 range from field tests. Most of the simulation results from this paper in three cases are also  
 300 within the range from field tests, except for the displacement of rail in case 1, in which the  
 301 static material properties are used. It is also noticeable that the simulation results from this  
 302 paper in all three cases are generally a little bit lower than the simulation results from Cai et al.  
 303 [47]. This is mainly caused by the different track irregularities. Both PSD and amplitude of  
 304 Qinhuangdao-Shenyang track irregularity are higher than the Germany low-disturbance  
 305 irregularity [48], so the Qinhuangdao-Shenyang track irregularity could cause a higher  
 306 excitation to train-track interactions, but the differences between two simulation models are  
 307 still acceptable. Another interesting phenomenon is that there are obvious differences in  
 308 vibration responses when the three types of material properties are used. These differences  
 309 can be attributable to various dynamic phenomena as previously found in other dynamic track  
 310 investigations [49-55]. In short, the simulation results from the model developed in this paper  
 311 exhibit a good agreement with the field test results and simulation results.

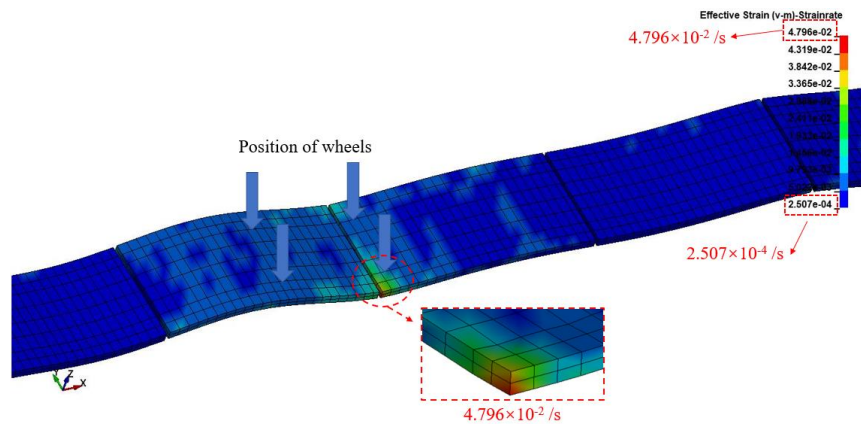
## 312 5. Results and discussion

313 In order to highlight the influence of the dynamic material properties of the slab track on  
 314 the vibration responses of train and track, the strain-rate enhancement effect for modulus of

315 elasticity of concrete and CA mortar under dynamic train loads is analyzed firstly. Then, the  
316 vibration responses of the vehicle, wheel-rail contact, and the track components are presented  
317 using three types of material properties: using static stiffness of rail pads and static modulus  
318 of elasticity of concrete and CA mortar (legend is named as using static properties for track  
319 components); using dynamic stiffness of rail pads and static modulus of elasticity of concrete  
320 and CA mortar (legend is named as using dynamic stiffness for rail pads); and using dynamic  
321 stiffness of rail pads and dynamic modulus of elasticity of concrete and CA mortar (legend is  
322 named as using dynamic properties for track components). And the deviation coefficients are  
323 calculated to present the effects of properties on train-track interactions.

### 324 5.1 Enhancement effects for the modulus of elasticity

325 The effective strain-rate is time-dependent when the vehicle is running along the track,  
326 so the dynamic moduli of elasticity of concrete and CA mortar are also time-dependent since  
327 the dynamic modulus of elasticity has the same distribution with the effective strain-rate.  
328 Figure 7 shows the contours of the distribution of the effective strain-rate of concrete slab and  
329 CA mortar when the maximum effective strain-rate occurs with the train speed of 400 km/h.  
330 The maximum effective strain-rates for concrete slab and CA mortar are  $4.796 \times 10^{-2}$  /s and  
331  $1.683 \times 10^{-1}$  /s, respectively, and they occur at the corner of the concrete slab and CA mortar, as  
332 shown in Figure 7. Note that although the minimum effective strain-rates of concrete slab and  
333 CA mortar in Figure 7 are  $2.507 \times 10^{-4}$  /s and  $2.082 \times 10^{-3}$  /s, respectively, they are just  
334 minimum values at one moment. The actual minimum values are static effective strain rates.

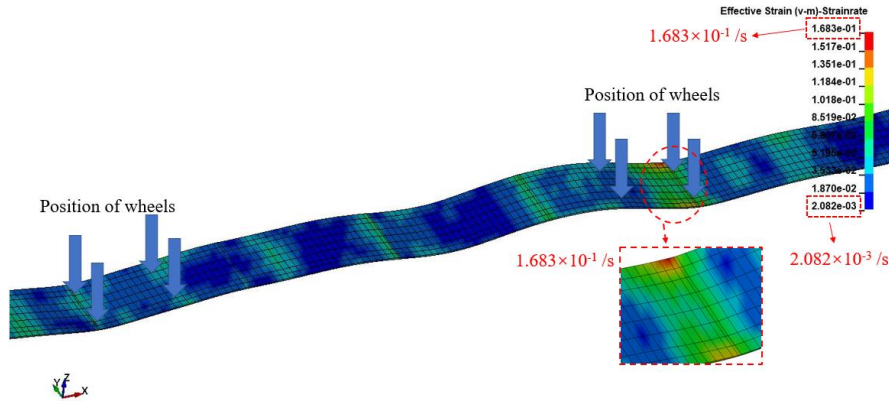


335

336

(a)





(b)

Figure 7 Contours of the effective strain-rate of the concrete slab and CA mortar at 400 km/h

(a) Concrete slab (b) CA mortar (max displacement factor=3000)

The maximum and minimum effective strain-rates of concrete slab, CA mortar, and concrete base under dynamic train loads with different train speeds (from 100 km/h to 400 km/h) are shown in Table 5. When the train speed is increased, the maximum effective strain-rate is increased obviously. For concrete, the magnitude of the maximum effective strain-rate does not increase much, but the maximum effective strain-rate of CA mortar increases significantly with train speeds. As for the minimum effective strain-rate, it is within the quasi-static range and does not change much with the train speed. The minimum effective strain-rates of concrete and CA mortar at these four train speeds are  $4.667 \times 10^{-6}$  /s and  $6.251 \times 10^{-5}$  /s, respectively.

Table 5 Maximum and minimum effective strain-rates of track components under dynamic train loads

		Train speeds	100 km/h	200 km/h	300 km/h	400 km/h
Maximum effective strain-rate (/s)	Concrete slab		$1.646 \times 10^{-2}$	$3.122 \times 10^{-2}$	$4.021 \times 10^{-2}$	$4.796 \times 10^{-2}$
	CA mortar		$7.671 \times 10^{-2}$	$7.457 \times 10^{-2}$	$1.231 \times 10^{-1}$	$1.683 \times 10^{-1}$
	Concrete base		$1.206 \times 10^{-2}$	$1.487 \times 10^{-2}$	$3.000 \times 10^{-2}$	$3.884 \times 10^{-2}$
Minimum effective strain-rate (/s)	Concrete slab		$4.667 \times 10^{-6}$	$9.121 \times 10^{-6}$	$9.186 \times 10^{-6}$	$6.054 \times 10^{-6}$
	CA mortar		$9.009 \times 10^{-5}$	$7.017 \times 10^{-5}$	$6.251 \times 10^{-5}$	$8.252 \times 10^{-5}$
	Concrete base		$8.524 \times 10^{-6}$	$1.479 \times 10^{-5}$	$8.252 \times 10^{-5}$	$1.061 \times 10^{-5}$

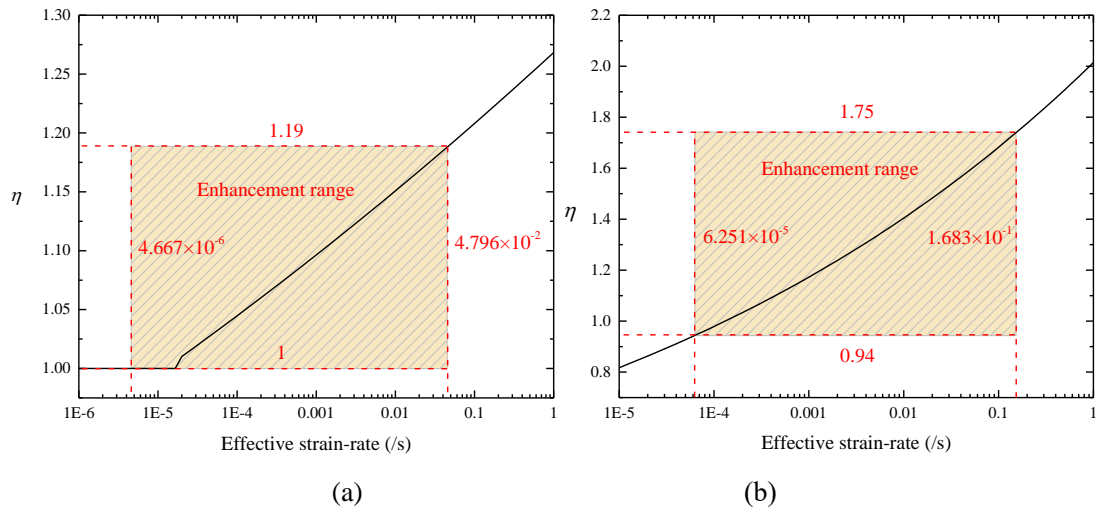
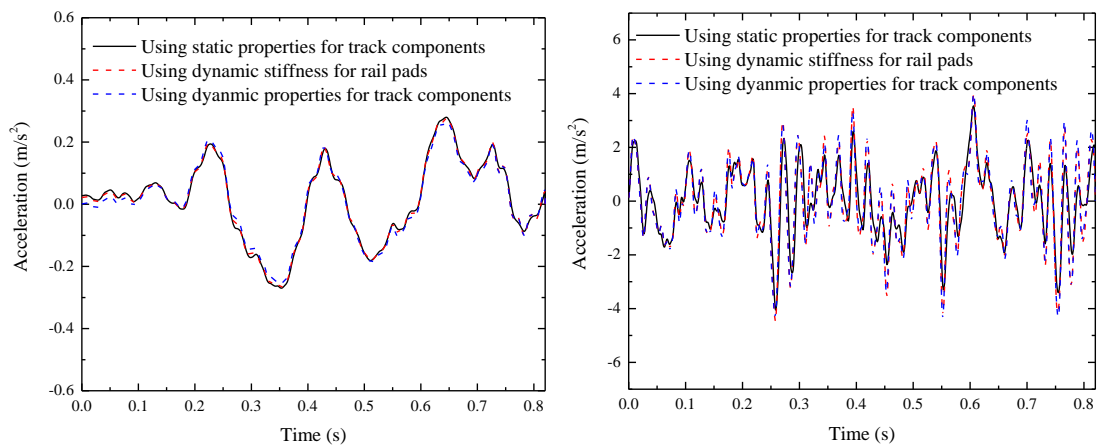
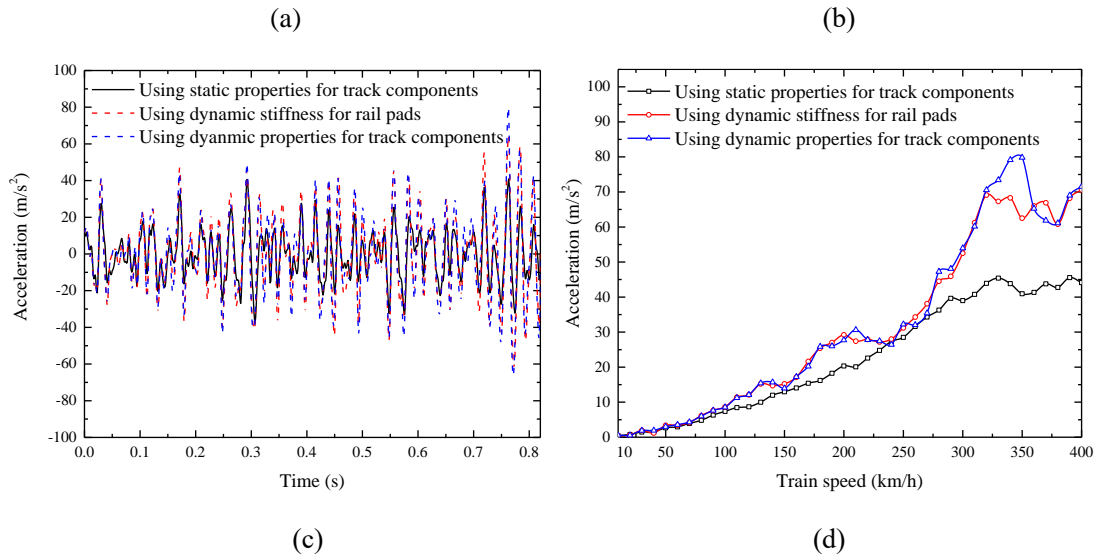


Figure 8 Enhancement range (a) Concrete (b) CA mortar

The enhancement range for dynamic moduli of elasticity of concrete and CA mortar can be determined from the maximum and minimum effective strain-rate, as shown in Figure 8. Since the effective strain-rate of concrete changes from  $4.667 \times 10^{-6}$  /s to  $4.796 \times 10^{-2}$  /s, the strain-rate enhancement factor for the modulus of elasticity of concrete changes from 1 to 1.19. And for CA mortar, the strain-rate enhancement factor changes from 0.94 to 1.75. This indicates that there will be at most 19% and 75% of amplification for the moduli of elasticity of concrete and CA mortar under dynamic train loads. Also, note that although the minimum effective strain-rates of concrete and CA mortar are determined from the values at four train speeds, they are quasi-static values, indicating that these values will not change much with train speeds and can represent the minimum effective strain-rates and minimum enhancement factors.

## 5.2 Effects on the vibration of the vehicle





370

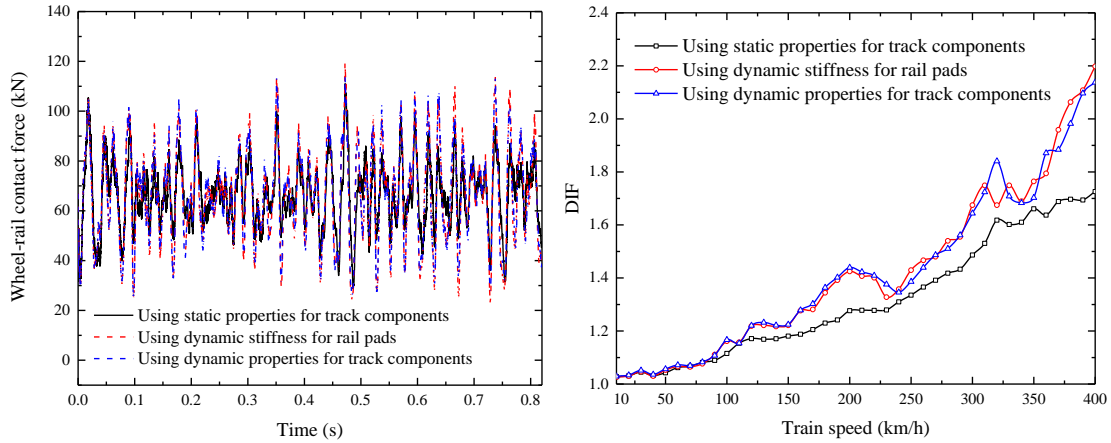
371

372 Figure 9 Vertical acceleration of the vehicle (a) Time history of the acceleration of car body at  
 373 350 km/h (b) Time history of the acceleration of bogie at 350 km/h (c) Time history of the  
 374 acceleration of wheelset at 350 km/h (d) Acceleration of the wheelset with train speeds

375 The influence of the material properties on the vibration acceleration of the vehicle is  
 376 shown in Figure 9. The dynamic material properties (both dynamic stiffness and dynamic  
 377 modulus of elasticity) have no significant influences on the acceleration of the car body, as  
 378 shown in Figure 9 (a), but they increase the amplitudes of the acceleration of the bogie and  
 379 wheelset obviously, as shown in Figure 9 (b) and (c). And there are no obvious differences in  
 380 the acceleration of the bogie and wheelset whether the dynamic modulus of elasticity is used  
 381 or not. Figure 9 (d) shows the relationship between the maximum acceleration of the wheelset  
 382 and the train speeds. When the train speed is no more than 70 km/h, the maximum  
 383 accelerations of the wheelset are quite similar either using static or dynamic material  
 384 properties of slab tracks because the low train speed cannot induce significant dynamic  
 385 excitation. However, once the train speed is higher than 70 km/h, the influence of the material  
 386 properties on the acceleration of the wheelset can be observed. The acceleration of the  
 387 wheelset is the lowest when the static material properties are used. And when the dynamic  
 388 stiffness of rail pads is used, the acceleration of the wheelset is increased obviously. In  
 389 addition, the influence of the dynamic modulus of the elasticity on the acceleration of the  
 390 wheelset is not significant at most of the train speeds. Moreover, it seems to be two resonant  
 391 peaks occurring in the acceleration of wheelset at all train speeds. One is at around 200 km/h,

392 and another is at around 320-360 km/h.

### 393 5.3 Effects on the wheel-rail contact force



394

Time (s)

(a)

395

(b)

396 Figure 10 Wheel-rail contact force (a) Time history of the wheel-rail contact force at 350  
397 km/h (b) DIF with train speeds

398 It is important to calculate the dynamic impact factor (DIF) based on the wheel-rail  
399 contact force for designing the slab track in railway engineering. The DIF is calculated as  
400 follows:

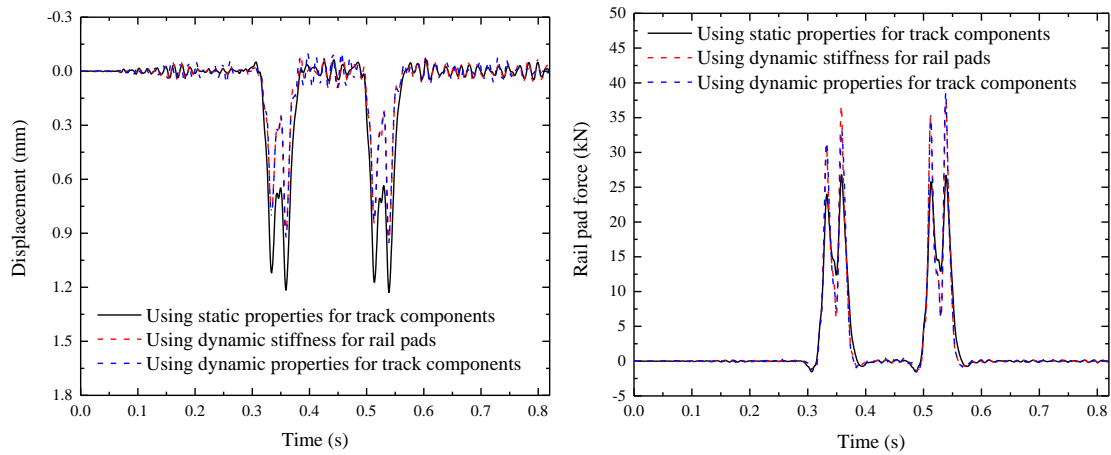
$$401 \text{DIF} = \frac{P_{\max}}{P_{\text{static}}} \quad (8)$$

402 Where  $P_{\max}$  is the maximum dynamic wheel-rail contact force, and  $P_{\text{static}}$  is the static  
403 wheel-rail contact force.

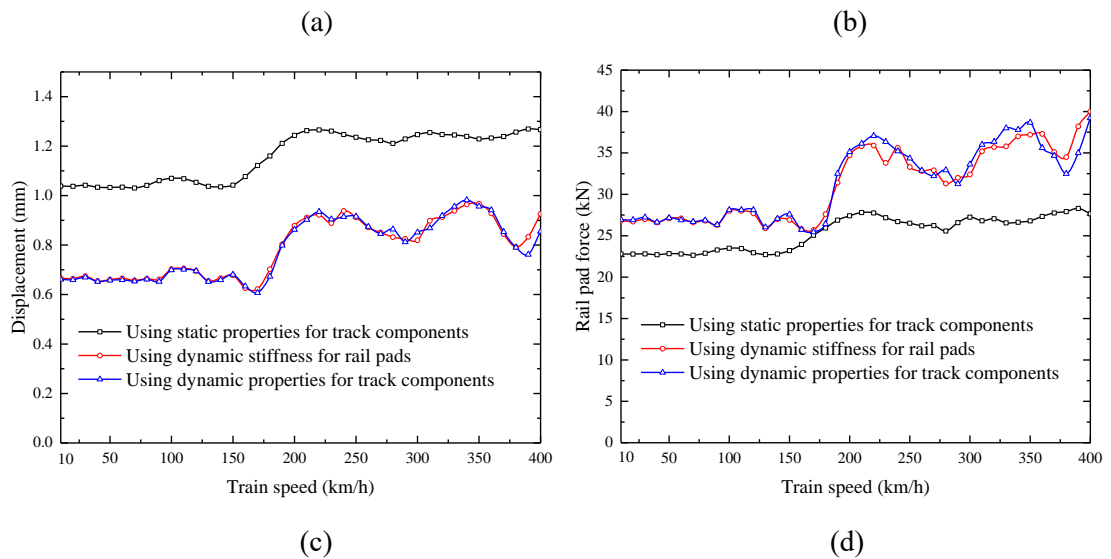
404 Figure 10 shows the effect of the material properties on the wheel-rail contact force.  
405 When the train speed is 350 km/h, the time history of wheel-rail contact force is shown in  
406 Figure 10 (a). The dynamic material properties (both dynamic stiffness and dynamic modulus  
407 of elasticity) could increase the amplitudes of the wheel-rail contact force, but the dynamic  
408 modulus of elasticity has no additional enlargement effect compared with the dynamic  
409 stiffness. Figure 10 (b) shows the relationship between the DIF and train speed. Similar to the  
410 acceleration of the wheelset, when the train speed is no more than 70 km/h, the material  
411 properties have no influences on the DIF. When the train speed is higher than 70 km/h, the  
412 DIF is the lowest with the static material properties. The dynamic stiffness of rail pads could

413 increase the DIF significantly, but the dynamic modulus of elasticity has little influences  
 414 compared with the dynamic stiffness of rail pads. Also, the two resonant peaks in DIF occur at  
 415 around 200 km/h and 320 km/h.

416 **5.4 Effects on the vibration of the rail**



417  
 418



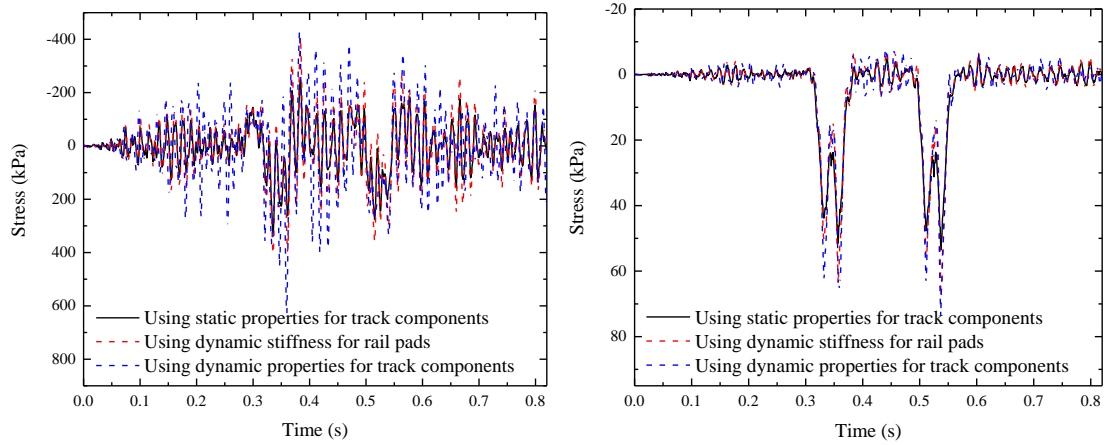
419  
 420

421 Figure 11 Dynamic responses of the rail (a) Time history of the vertical displacement of rail at  
 422 350 km/h (b) Time history of the vertical rail pad force at 350 km/h (c) Displacement of the  
 423 rail with train speeds (d) Rail pad force with train speeds

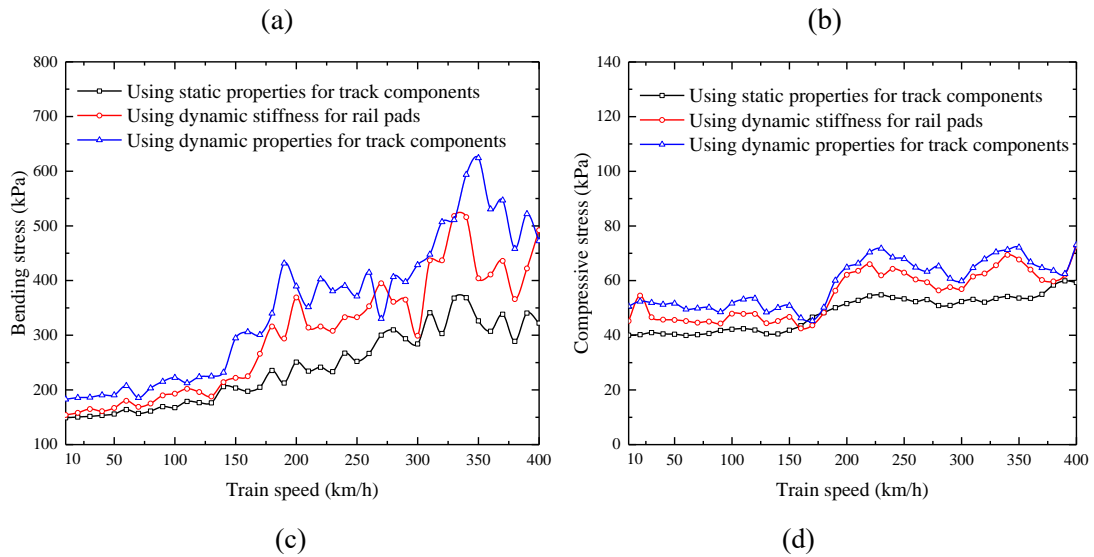
424 Figure 11 shows the effects of the material properties on the vertical displacement of the  
 425 rail and the rail pad force. When the train speed is 350 km/h, the maximum displacement of  
 426 the rail using dynamic material properties is much lower than that using static properties, and  
 427 the dynamic modulus of elasticity still has little influences compared with the dynamic  
 428 stiffness, as shown in Figure 11(a). In contrast, the rail pad force using dynamic properties is

429 much higher than that using static properties, as shown in Figure 11(b). This phenomenon can  
 430 also be observed at all train speeds, as shown in Figure 11 (c) and (d). And the resonant peaks  
 431 using static properties seem to occur at 210 km/h and 320 km/h. When the dynamic properties  
 432 are used, the peaks move to the right side at 220 km/h and 330 km/h.

433 **5.5 Effects on the vibration of the concrete slab and CA mortar**



434  
 435



436  
 437

438 Figure 12 Dynamic stress of the slab track components (a) Time history of the bending stress  
 439 of the concrete slab at 350 km/h (b) Time history of the compressive stress of the CA mortar  
 440 at 350 km/h (c) Bending stress of the concrete slab with train speeds (d) Compressive stress  
 441 of the CA mortar with train speeds

442 The concrete slab mainly undertakes bending moments under dynamic train loads. Thus  
 443 the bending stress is the dominant stress for concrete slab. Also, the CA mortar mainly bears  
 444 compressive loads, so that the compressive stress is the highest stress for CA mortar. When

445 the train speed is 350 km/h, the time history of the bending stress of the concrete slab and the  
 446 compressive stress of CA mortar with three types of material properties are shown in Figure  
 447 12 (a) and (b). Unlike the effect of the dynamic modulus of elasticity on the acceleration of  
 448 the vehicle, wheel-rail contact force, and vibration of the rail, the dynamic modulus of  
 449 elasticity has a significant influence on the stress of the concrete slab and CA mortar. When  
 450 the dynamic stiffness of rail pads is used, the maximum bending and compressive stress are  
 451 increased. When the dynamic modulus of elasticity is considered, the bending and  
 452 compressive stresses are increased furthermore. This can also be observed at all train speeds,  
 453 as shown in Figure 12 (c) and (d).

## 454 5.6 Deviation coefficients

455 In order to investigate the deviation of the vibration responses of the train-track  
 456 interactions induced by either static or dynamic material properties, the three deviation  
 457 coefficients are calculated as follows:

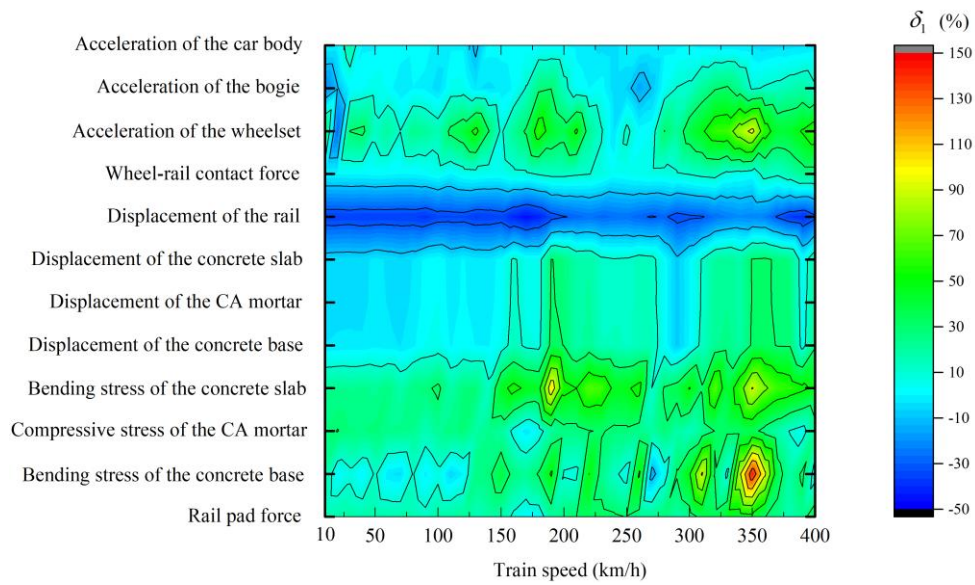
$$458 \quad \delta_1 = \left( \frac{P_{dynamic} - P_{static}}{P_{static}} \right) \times 100\% \quad (9)$$

$$459 \quad \delta_2 = \left( \frac{P_{dyn-stiffness} - P_{static}}{P_{static}} \right) \times 100\% \quad (10)$$

$$460 \quad \delta_3 = \left( \frac{P_{dynamic} - P_{dyn-stiffness}}{P_{static}} \right) \times 100\% \quad (11)$$

461 Where  $\delta_1$  is the deviation coefficient which presents the deviation of vibration responses  
 462 induced by the dynamic stiffness of rail pads and dynamic moduli of elasticity of concrete and  
 463 CA mortar compared with the static material properties;  $\delta_2$  is the deviation coefficient which  
 464 presents the deviation of vibration responses induced by the dynamic stiffness of rail pads  
 465 compared with the static material properties;  $\delta_3$  is the deviation coefficient which presents the  
 466 deviation of vibration responses induced by the dynamic moduli of elasticity of concrete and  
 467 CA mortar compared with the static material properties;  $P_{dynamic}$  is the maximum vibration  
 468 responses considering both dynamic stiffness and dynamic modulus of elasticity;  $P_{static}$  is the  
 469 maximum vibration responses using static material properties; and  $P_{dyn-stiffness}$  is the maximum

470 vibration responses using dynamic stiffness for rail pads.



471

472 **Figure 13 Contour of the deviation coefficient**

473 Figure 13 shows the distribution of the deviation coefficient ( $\delta_1$ ). The maximum  
 474 deviation coefficient occurs at 350 km/h in bending stress of the concrete base, and this might  
 475 be induced by the resonance of the train-track interactions. The minimum deviation  
 476 coefficient occurs in the displacement of the rail, which is negative because the displacement  
 477 of the rail using dynamic properties is lower than that using static properties. For all of the  
 478 vibration responses, the deviation coefficients are still pronounced at around 200 km/h and  
 479 350 km/h because of the resonance.

480

Table 6 Deviation coefficients at 350 km/h

Components	$\delta_1$ (%)	$\delta_2$ (%)	$\delta_3$ (%)
Acceleration of the car body	-3.82	-1.74	-2.08
Acceleration of the bogie	8.33	9.36	-1.03
Acceleration of the wheelset	95.06	52.68	42.37
Wheel-rail contact force	2.54	6.24	-3.70
Rail pad force	44.33	38.84	5.50
Displacement of the rail	-22.19	-21.31	-0.88
Displacement of the concrete slab	30.98	30.56	0.42
Displacement of the CA mortar	30.73	30.57	0.16
Displacement of the concrete base	31.79	30.77	1.02



Bending stress of the concrete slab	91.32	23.82	67.50
Compressive stress of the CA mortar	34.67	26.33	8.34
Bending stress of the concrete base	144.36	29.89	114.47

481 Table 6 shows the three deviation coefficients at 350 km/h. The maximum deviation  
482 coefficient between static and dynamic material properties ( $\delta_1$ ) is 144.36% in the bending  
483 stress of the concrete base. The effects of the material properties on the acceleration of the  
484 wheelset and the bending stress of the slab are also pronounced since the  $\delta_1$  equals to 95.06%  
485 and 91.32%, respectively. The deviation coefficients of  $\delta_2$  are quite high on the displacement  
486 of the track components and rail pad force, indicating the dynamic stiffness of rail pads makes  
487 a significant contribution to these responses. The deviation coefficient of  $\delta_3$  accounts for a  
488 large proportion on the dynamic stress of the track components, indicating the dynamic  
489 modulus of elasticity has a significant influence on the dynamic stress of the track  
490 components.

## 491 6. Conclusions

492 Most train-track interaction studies have merely considered only static and quasi-static  
493 properties of materials. Despite the use of field data to tune the values of the material  
494 properties for model validations and agreements, the fundamental body of knowledge is  
495 unclear and questionable. In order to investigate the influences of the dynamic material  
496 properties on the train-track vibration interactions, the coupled vehicle-track numerical model  
497 has been developed based on the multi-body simulation principle and finite element theory in  
498 LS-DYNA with three types of material properties: static stiffness for rail pads and static  
499 moduli of elasticity for concrete and CA mortar, dynamic stiffness for rail pads and static  
500 moduli of elasticity for concrete and CA mortar, and dynamic stiffness for rail pads and  
501 strain-rate-dependent moduli for concrete and CA mortar. The model has been validated by  
502 comparing the results with the field test results and other simulations results, and a good  
503 agreement has been found. The following conclusions can be drawn:

504 (a) When the strain-rate-dependent moduli of elasticity of concrete and CA mortar are  
505 considered, the dynamic moduli of concrete and CA mortar are increased by at most 19% and

506 75% under dynamic train loads.

507 (b) When the train speed is no more than 70 km/h, the effect of material properties does  
508 not need to be considered for the vibration of the vehicle and wheel-rail contact force. In  
509 contrast, when the train speed is higher than 70 km/h, the dynamic material properties have a  
510 significant influence on the train-track vibration interactions.

511 (c) The maximum bending stress of the concrete base is increased by at most 114.36%  
512 when the dynamic material properties are used. The effect of material properties on the  
513 acceleration of the wheelset and the bending stress of concrete slab is also pronounced,  
514 although such effect on the acceleration of the car body and bogie is rather little.

515 (d) The stiffness of rail pads has the dominant influence on the train-track vibrations, and  
516 the dynamic modulus mainly affects the vibration stress of the track components. So the  
517 dynamic stiffness of rail pads should be considered in simulations in all cases, and the  
518 dynamic modulus of elasticity of concrete and CA mortar could be considered depends on the  
519 analysis purpose under normal track irregularities.

## 520 **Acknowledgments**

521 This research was supported by the Key Research Development Program of China  
522 (No.2016YFC0802203-2, No.2016YFC0802203-3). The authors would like to acknowledge  
523 the China Scholarship Council for the financial support. The authors sincerely thank  
524 European Commission for H2020-MSCA-RISE Project No. 691135 “RISEN: Rail  
525 Infrastructure Systems Engineering Network,” which enables a global research network that  
526 tackles the grand challenge in railway infrastructure resilience and advanced sensing under  
527 extreme conditions ([www.risen2rail.eu](http://www.risen2rail.eu)) [56]. Technical assistance by Dr Keiichi Goto is  
528 gratefully acknowledged.

## 529 **References**

- 530 [1] Esveld C. Recent developments in slab track[J]. European railway review, 2003, 9(2): 81-85.  
531 [2] Zhai W, Han Z, Chen Z, et al. Train-track-bridge dynamic interaction: a state-of-the-art  
532 review[J]. Vehicle System Dynamics, 2019: 1-44.

- 533 [3] Ren J, Deng S, Wei K, et al. Mechanical property deterioration of the prefabricated concrete  
534 slab in mixed passenger and freight railway tracks[J]. Construction and Building Materials,  
535 2019, 208: 622-637.
- 536 [4] Li T, Su Q, Shao K, et al. Numerical Analysis of Vibration Responses in High-Speed  
537 Railways considering Mud Pumping Defect[J]. Shock and Vibration, 2019, 2019.
- 538 [5] Zhai W, Wei K, Song X, et al. Experimental investigation into ground vibrations induced by  
539 very high speed trains on a non-ballasted track[J]. Soil Dynamics and Earthquake  
540 Engineering, 2015, 72: 24-36.
- 541 [6] Zhu S, Cai C. Stress intensity factors evaluation for through-transverse crack in slab track  
542 system under vehicle dynamic load[J]. Engineering Failure Analysis, 2014, 46: 219-237.
- 543 [7] Wang M, Cai C, Zhu S, et al. Experimental study on dynamic performance of typical  
544 nonballasted track systems using a full-scale test rig[J]. Proceedings of the Institution of  
545 Mechanical Engineers, Part F: Journal of Rail and Rapid Transit, 2017, 231(4): 470-481.
- 546 [8] Lin H, Liu X, Yan H, et al. Long-Term Behavior and Performance of Ballastless Track  
547 Superstructure on China's Suining-Chongqing Railway Line[C]//2010 Joint Rail Conference.  
548 American Society of Mechanical Engineers, 2010: 299-303.
- 549 [9] Kaewunruen S, Remennikov A M. Experiments into impact behaviour of railway prestressed  
550 concrete sleepers[J]. Engineering Failure Analysis, 2011, 18(8): 2305-2315.
- 551 [10] Alexandrou G, Kouroussis G, Verlinden O. A comprehensive prediction model for  
552 vehicle/track/soil dynamic response due to wheel flats[J]. Proceedings of the Institution of  
553 Mechanical Engineers, Part F: Journal of Rail and Rapid Transit, 2016, 230(4): 1088-1104.
- 554 [11] Kaewunruen S, Remennikov A M. Field trials for dynamic characteristics of railway track  
555 and its components using impact excitation technique[J]. Ndt & E International, 2007, 40(7):  
556 510-519.
- 557 [12] Chen X, Wu S, Zhou J. Experimental and modeling study of dynamic mechanical properties  
558 of cement paste, mortar and concrete[J]. Construction and Building Materials, 2013, 47:  
559 419-430.
- 560 [13] Kaewunruen S, Remennikov A M. An alternative rail pad tester for measuring dynamic  
561 properties of rail pads under large preloads[J]. Experimental Mechanics, 2008, 48(1): 55-64.
- 562 [14] Tian Y, Cheng Y.R. and Liu X.W. Studies on the dynamic behaviour of U71Mn rail steel

563 under high strain rate, China Railway Science, 1992, 13, 34-42. (In Chinese).

564 [15] Bischoff P H, Perry S H. Compressive behaviour of concrete at high strain rates[J]. Materials  
565 and structures, 1991, 24(6): 425-450.

566 [16] Kaewunruen S, Wang Y, Ngamkhanong C. Derailment-resistant performance of modular  
567 composite rail track slabs[J]. Engineering Structures, 2018, 160: 1-11.

568 [17] Kaewunruen S, Remennikov A M. Impact capacity of railway prestressed concrete  
569 sleepers[J]. Engineering Failure Analysis, 2009, 16(5): 1520-1532.

570 [18] Ngamkhanong C, Li D, Remennikov A M, et al. Dynamic capacity reduction of railway  
571 prestressed concrete sleepers due to surface abrasions considering the effects of strain rate  
572 and prestressing losses[J]. International Journal of Structural Stability and Dynamics, 2019,  
573 19(01): 1940001.

574 [19] Xie Y, Fu Q, Zheng K, et al. Dynamic mechanical properties of cement and asphalt mortar  
575 based on SHPB test[J]. Construction and Building Materials, 2014, 70: 217-225.

576 [20] Chen X, Wu S, Zhou J. Experimental and modeling study of dynamic mechanical properties  
577 of cement paste, mortar and concrete[J]. Construction and Building Materials, 2013, 47:  
578 419-430.

579 [21] Yongliang L, Xiangming K, Yanrong Z, et al. Static and dynamic mechanical properties of  
580 cement-asphalt composites[J]. Journal of Materials in Civil Engineering, 2012, 25(10):  
581 1489-1497.

582 [22] Lee O S, Kim M S. Dynamic material property characterization by using split Hopkinson  
583 pressure bar (SHPB) technique[J]. Nuclear Engineering and Design, 2003, 226(2): 119-125.

584 [23] Zeng X H, Xie Y J, Deng D H, et al. A study of the dynamic mechanical properties of CRTS I  
585 type CA mortar[J]. Construction and Building Materials, 2016, 112: 93-99.

586 [24] Kaewunruen S, Remennikov A M. Sensitivity analysis of free vibration characteristics of an  
587 in situ railway concrete sleeper to variations of rail pad parameters[J]. Journal of Sound and  
588 Vibration, 2006, 298(1-2): 453-461.

589 [25] Sol-Sánchez M, Moreno-Navarro F, Rubio-Gámez M C. The use of elastic elements in  
590 railway tracks: A state of the art review[J]. Construction and building materials, 2015, 75:  
591 293-305.

592 [26] Wei K, Yang Q, Dou Y, et al. Experimental investigation into temperature-and

593 frequency-dependent dynamic properties of high-speed rail pads[J]. Construction and  
594 Building Materials, 2017, 151: 848-858.

595 [27] Zhai W, Wang K, Cai C. Fundamentals of vehicle-track coupled dynamics[J]. Vehicle System  
596 Dynamics, 2009, 47(11): 1349-1376.

597 [28] Chen Z, Zhai W, Yin Q. Analysis of structural stresses of tracks and vehicle dynamic  
598 responses in train-track-bridge system with pier settlement[J]. Proceedings of the Institution  
599 of Mechanical Engineers, Part F: Journal of Rail and Rapid Transit, 2018, 232(2): 421-434.

600 [29] Xu G.H., Zhang H.P., Huang H., et al. Discussion on testing method of fastener products  
601 mechanical performance of urban rail transit[J]. Shanxi Architecture,  
602 2016,42(13):159-161.(In Chinese).

603 [30] CEB Bulletin Number 182, Concrete structures under impact and impulsive  
604 loading-Synthesis Report; 1988.

605 [31] Birmann F. Recent investigations of the dynamic modulus of elasticity of the track in ballast  
606 with regard to high speeds[M]//Railroad Track Mechanics and Technology. Pergamon, 1978:  
607 197-221.

608 [32] Zhai W, Han Z, Chen Z, et al. Train-track-bridge dynamic interaction: a state-of-the-art  
609 review[J]. Vehicle System Dynamics, 2019: 1-44.

610 [33] Zhu S, Cai C. Stress intensity factors evaluation for through-transverse crack in slab track  
611 system under vehicle dynamic load[J]. Engineering Failure Analysis, 2014, 46: 219-237.

612 [34] Zhu S, Yang J, Yan H, et al. Low-frequency vibration control of floating slab tracks using  
613 dynamic vibration absorbers[J]. Vehicle System Dynamics, 2015, 53(9): 1296-1314.

614 [35] Xu L, Zhai W. A new model for temporal-spatial stochastic analysis of vehicle-track coupled  
615 systems[J]. Vehicle System Dynamics, 2017, 55(3): 427-448.

616 [36] Sun L, Chen L, Zelelew H H. Stress and deflection parametric study of high-speed railway  
617 CRTS-II ballastless track slab on elevated bridge foundations[J]. Journal of Transportation  
618 Engineering, 2013, 139(12): 1224-1234.

619 [37] Zhai W, Liu P, Lin J, et al. Experimental investigation on vibration behaviour of a CRH train  
620 at speed of 350 km/h[J]. International Journal of Rail Transportation, 2015, 3(1): 1-16.

621 [38] Lei X, Wang J. Dynamic analysis of the train and slab track coupling system with finite  
622 elements in a moving frame of reference[J]. Journal of Vibration and Control, 2014, 20(9):

623 1301-1317.

624 [39] Juanjuan R, Rongshan Y, Ping W, et al. Influence of contact loss underneath concrete  
625 underlayer on dynamic performance of prefabricated concrete slab track[J]. Proceedings of  
626 the Institution of Mechanical Engineers, Part F: Journal of Rail and Rapid Transit, 2017,  
627 231(3): 345-358.

628 [40] Wei K, Wang F, Wang P, et al. Effect of temperature-and frequency-dependent dynamic  
629 properties of rail pads on high-speed vehicle-track coupled vibrations[J]. Vehicle System  
630 Dynamics, 2017, 55(3): 351-370.

631 [41] Jiang H, Chorzepa M G. An effective numerical simulation methodology to predict the  
632 impact response of pre-stressed concrete members[J]. Engineering Failure Analysis, 2015, 55:  
633 63-78.

634 [42] Schwer L. The Winfrith concrete model: Beauty or beast? Insights into the Winfrith concrete  
635 model[C]//8th European LS-DYNA Users Conference. 2011: 23-24.

636 [43] Ren J.J., Xu J.D., Tian G.Y., et al. Field test and statistical characteristics of wheel-rail force  
637 for slab track with passenger and freight traffic[J]. Engineering Mechanics, 2018,35(02):239-248.(In Chinese).

638

639 [44] Nan H.Y. Analysis on the dynamic characteristics of CRTS II type slab ballastless track on  
640 subgrade and parametric study[D]. Lanzhou Jiaotong University, 2012. (In Chinese).

641 [45] Yan. S.C. Test study on subgrade load performance and the road-culvert transition  
642 performance in Suiyu railway[D]. Southwest Jiaotong University, 2007.(In Chinese).

643 [46] Zhan J.X., Jiang G.L., Hu A.H., et al. Study of dynamic response of pile-plank embankment  
644 of ballastless track based on field test in Suining-Chongqing High-speed Railway[J]. Rock  
645 and Soil Mechanics, 2009,30(03):832-835. (In Chinese).

646 [47] Cai C.B., Zhai W.M., and Wang K.Y. Calculation and Assessment Analysis of the Dynamic  
647 Performance for Slab Track on Sui-Yu Railway[J]. China Railway Science, 2006(04):17-21.  
648 (In Chinese).

649 [48] Wang K.Y., Zhai W.M., and Cai C.B. Comparison on track spectra of  
650 Qinhuangdao-Shenyang passenger railway line and German railway line[J]. Journal of  
651 Southwest Jiaotong University, 2007(04):425-430. (In Chinese).

652 [49] Griffin D.W.P., Mirza O, Kwok K, and Kaewunruen S. Composite slabs for railway  
653 construction and maintenance: a mechanistic review[J]. The IES Journal Part A: Civil &

654 Structural Engineering, 2014(7): 243-262.

655 [50] Kaewunruen S. and Remennikov A.M. An alternative rail pad tester for measuring dynamic  
656 properties of rail pads under large preloads [J]. *Experimental Mechanics*, 2008(48): 55-64.

657 [51] Kaewunruen S. and Remennikov A.M. Current state of practice in railway track vibration  
658 isolation: an Australian overview[J]. *Australian Journal of Civil Engineering*, 2016(14):  
659 63-71.

660 [52] Kaewunruen S. and Kimani S.K. Damped frequencies of precast modular steel-concrete  
661 composite railway track slabs, *Steel and Composite Structures*, 2017, 25 (4), 427-442

662 [53] Kimani S.K. and Kaewunruen S. Free vibrations of precast modular steel-concrete composite  
663 railway track slabs, *Steel and Composite Structures*, 2017, 24 (1), 113-128.

664 [54] Mirza O. and Kaewunruen S. Resilience and Robustness of Composite Steel and Precast  
665 Concrete Track Slabs Exposed to Train Derailments. *Front. Built Environ.* 2018, 4:60. doi:  
666 10.3389/fbuil.2018.00060

667 [55] Kaewunruen S, Sussman JM and Einstein HH (2015) Strategic framework to achieve  
668 carbon-efficient construction and maintenance of railway infrastructure systems. *Front.*  
669 *Environ. Sci.* 3:6. doi: 10.3389/fenvs.2015.00006

670 [56] Kaewunruen S, Sussman JM and Matsumoto A (2016) Grand Challenges in Transportation  
671 and Transit Systems. *Front. Built Environ.* 2:4. doi: 10.3389/fbuil.2016.00004